Non-reciprocity in optical fiber links: experimental evidence

Dan Xu, Olivier Lopez, Anne Amy-Klein, Paul-Eric Pottie

Non-reciprocity in optical fiber links: experimental evidence

DAN XU,[1,2] **OLIVIER LOPEZ,**[2] **ANNE AMY-KLEIN,**[2] **AND PAUL-ERIC POTTIE**[1,*]

[1]*LNE-SYRTE, Observatoire de Paris, Université PSL, CNRS, Sorbonne Université, 61 Avenue de l'Observatoire, 75014 Paris, France*
[2]*Laboratoire de Physique des Lasers, Université Sorbonne Paris Nord, CNRS, 99 Avenue Jean-Baptiste Clément, 93430 Villetaneuse, France*
*paul-eric.pottie@obspm.fr

Abstract: Fundamental limits of fiber link are set by non-reciprocal effects that violate the hypothesis of equality between forward and backward path. Non-reciprocal noise arises technically from the set-up asymmetry, and fundamentally by the Sagnac effect when the fiber link encloses a non-zero area. As a pre-requisite for observation of Sagnac effect in fiber links, we present a study on phase noise and frequency stability contributions affecting coherent optical frequency transfer in bi-directional fiber links. Both technical and fundamental limitations of Two-Way optical frequency transfer are discussed. Our model predicts and our experiments substantially verify that the dominant noise mechanism at low Fourier frequencies is the polarization asymmetry induced by the temperature and relative humidity variations impacted on fiber links. The flicker noise floor due to the non-reciprocal noise arising from polarization mode dispersion is evidenced for the first time. We perform a post-processing approach which enables us to remove this polarization noise, improve the long-term stability and remove a frequency bias. We evaluate the uncertainty contributions of all the effects discussed for our 50 km spooled fiber link, dominated by its non-reciprocal noise induced by polarization mode dispersion with uncertainty of $1.9(\pm 0.8)(\pm 1.2) \times 10^{-20}$. After correction, the linear drift of the residual phase is as low as 27 yoctosecond/s, leading to an uncertainty of the frequency transfer of $2.6 (\pm 39) \times 10^{-22}$, confirming its potential for searching for more fundamental effects such as Sagnac effect or transient frequency variation due to dark matter.

1. Introduction

Optical fiber links play an important role in today global efforts towards a redefinition of the International System of Units (SI) second and coordination of international atomic time. Using a specialized optical frequency transfer system over optical fiber that compensated actively for the propagation delay fluctuations [1], people were able to compare the frequencies of their atomic clocks located in the National Metrological Institutes all around the world [2–8]. With the development of ultra-accurate atomic clocks with instability of $2 \times 10^{-16}(\tau/s)^{-1/2}$ for averaging time τ [9], and even lower instability of $4.8 \times 10^{-17}(\tau/s)^{-1/2}$ [10], highly stable fiber links become increasingly important to make full use of the clock stability.

Fiber links operated in the optical frequency domain use an ultra-stable laser as a frequency signal. This signal is degraded by the propagation delay fluctuations, induced by thermal and mechanical perturbations that act on the fiber optical length, that is both on the physical length and the fiber refraction index. Although some actively or passively compensation techniques have been adopted to suppress these environmentally-induced optical phase noise [11–13], a fine understanding of the phase noise contributions will improve the use of fiber links and may widen its field of applications, such as study of Sagnac effect [14], search for dark matter [15–17] and quantum key distribution (QKD) [7].

In 2007-2008, a similar study on the performance limitations for optical frequency transport through long optical fiber links was performed, including measurement-related effects such as phase noise on the source, RF electronics, and receiver/transmitter interferometers, as well as link-related effects such as delay, non-linear effects, and polarization-mode dispersion [11]. The delay non-suppressed noise, which is a fundamental limit, dominates for high frequencies. Moreover, the fluctuations of the reference arms of the Michelson interferometer ensemble leads to so-called interferometer noise and bias, as the optical length of the reference arms varies with temperature fluctuations. The interferometer noise thus dominates for lower frequencies and usually varies as $1/f^2$. More recently, the interferometer noise was measured directly, but was found to vary as $1/f^3$ instead of $1/f^2$ [18,19]. This interferometer noise was largely rejected by post data-processing for in-field implementation, resulting in long-term instability improvement to 10^{-21} [19].

The perfect noise cancellation of bidirectional fiber experiments is based on the assumption that the forward and backward signals transferred on the fiber are exactly the same. For given identical polarization, power and frequency, light travels into non dispersive media reciprocally by law of reverse path of light. In practice, these assumptions are violated as the frequencies and powers are slightly different, the polarizations are crossed, and the fiber is birefringent. So beyond the limit set by the finite velocity of light, fundamental limits of fiber link are set by non-reciprocal effects. Non-reciprocal noise arises technically from the set-up asymmetry (either power, polarization or frequency), and fundamentally by the Sagnac effect when the fiber link encloses a non-zero area. We develop in this paper the theoretical analysis for the fundamental limits for fiber-based frequency transfer and optical clock comparison, and evaluate how much the performance of a fiber link is degraded by the path, frequency, wavelength and polarization asymmetry for the forward and backward signal transmitted on the optical fiber. We will discuss these asymmetries in details and report their limiting levels. Especially, the effect due to the fiber's birefringence, that alters the optical delay as a function of the polarization, is difficult to assess due to its small magnitude in the in-field telecommunication fiber network. A study recently reported experimental data using dual-polarization detection techniques that evidenced the dependency of the delay with the input polarization state of the reference laser field [7]. Here, we establish a simple yet powerful platform with fiber spools, so that the laser-field polarization rotation in the propagation media is strengthen by the mechanical constraints applied on the fiber. We demonstrate that, for the first time, the polarization mode dispersion, which induces non-reciprocal delay, dominates the residual phase fluctuations at lower frequencies when the interferometer noises are actively minimized.

2.   Experimental setup

Our setup of two-way optical frequency comparison is shown on Fig. 1. It is installed in two different labs connected by a 200 m duplex fiber. We used one pair of ~25 km optical spooled fibers in Lab2 that are connected as a loop, such that the local portion and remote portion of the setup are both located in Lab1. In Lab1, the ultra-stable optical frequency source at 1542 nm is split and fed into the fiber loop in each direction, while the remaining radiations served as local references. We used four Acousto-Optic Modulators (AOMs) to distinguish the signals coming from the stray reflections and distinguish the beat notes carrying on different segments of fiber noise. Two bi-directional Erbium-Doped Fiber Amplifiers (bi-EDFAs) are used to compensate the transmission loss without degrading the link performance [20]. At each direction, a coupler and a Faraday Mirror (FM) are used to build a strongly unbalanced Michelson interferometer to detect the beat notes which carry on the fiber noise [21]. The interferometer ensemble is a two-branch Michelson interferometer with a length mismatch of 0.15 m. The interferometer ensemble is described in details in Ref. [18]. In this present experiment, the interferometer ensemble is actively stabilized in temperature with a proportional-integral servo loop. The temperature of the

ensemble is measured with two probes out of loop and show residual fluctuations of <10 mK over 30 days. A Polarization Controller (PC) is used to optimize the amplitudes of the beat notes. All the beat notes detected on photodiodes (PD1 and PD2) are then filtered, tracked, simultaneously recorded by a dead-time free frequency counter operated in Π-type and Λ-type with 1 s gate time. Temperature in Lab1 and Lab2, as well as the temperature of the interferometer ensemble, are sensed with 10 kOhm thermal resistances. Humidity in Lab1 and Lab2 are sensed with a humidity sensor HTM2500LF. The data are logged with a datalogger every 10 s.
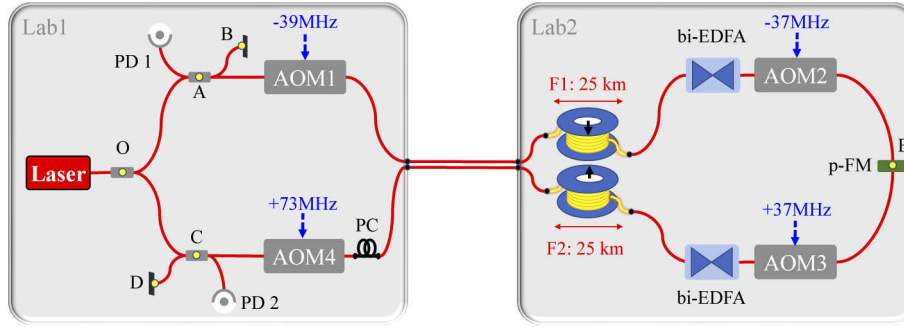

Fig. 1. Experiment setup. AOM, acousto-optic modulator; PD, photodiode; bi-EDFA, bi-directional erbium-doped fiber amplifier; p-FM, partial Faraday mirror; PC, polarization controller.

In this implementation, the optical signals propagating from fiber 1 (F1) to fiber 2 (F2) and from F2 to F1 are denoted with subscript $1 + 2$ and $2 + 1$. By using a partial Faraday Mirror (p-FM) in the middle of the fiber loop, with ratio of transmission:reflection = 50:50, we can obtain one more beat note both on PD1 and PD2, the round-trip (RT) signal on F1 and the round-trip signal on F2, denoted with subscript $1 + 1$ and $2 + 2$. The total phase evolution for these four beat notes can be written as:

$$
\begin{cases}
\Phi_{1+2} = \int_0^{L_1} \delta\phi(z, t - \tau_2 - (\tau_1 - z/v))dz + \int_0^{L_2} \delta\phi(z, t - z/v)dz, \\
\Phi_{2+1} = \int_0^{L_2} \delta\phi(z, t - \tau_1 - (\tau_2 - z/v))dz + \int_0^{L_1} \delta\phi(z, t - z/v)dz, \\
\Phi_{1+1} = \int_0^{L_1} \delta\phi(z, t - \tau_1 - (\tau_1 - z/v))dz + \int_0^{L_1} \delta\phi(z, t - z/v)dz, \\
\Phi_{2+2} = \int_0^{L_2} \delta\phi(z, t - \tau_2 - (\tau_2 - z/v))dz + \int_0^{L_2} \delta\phi(z, t - z/v)dz.
\end{cases}
\tag{1}
$$

where v is the speed of light in the fiber, L_1 and L_2 are the length of F1 and F2, $\tau_1 = L_1/v$ and $\tau_2 = L_2/v$ are their propagation delays, and $\delta\phi$ is the phase noise per unit of length at coordinate z and time t [22].

There is one more special beat note formed on p-FM between the forward signals from Lab1 to Lab2 on F1 and F2, denoted with subscript $2 - 1$, propagating back to Lab1 and detected on PD2. This beat note can be written as:

$$
\Phi_{2\text{-}1} = \int_0^{L_2} \delta\phi(z, t - \tau_2 - (\tau_2 - z/v))dz - \int_0^{L_1} \delta\phi(z, t - \tau_2 - (\tau_1 - z/v))dz.
\tag{2}
$$

From the frequency measurements made on PD1 and PD2, we can obtain 8 two-way (TW) observables [18,19] including in-situ noise floor.

Here we focus on the classical two-way (CTW) observable,

$$
\Phi_{\text{CTW}} = \Phi_{1+2} - \Phi_{2+1},
\tag{3}
$$

and one of the noise floor (NF) in-situ which is free of interferometer noise and non-reciprocal noise [18],

$$
\Phi_{\text{NF}} = \Phi_{1+1} + \Phi_{2+2} - \Phi_{1+2} - \Phi_{2+1} = 0.
\tag{4}
$$

As the two ends of the setup are set in the same lab, it avoids the necessity to exchange and synchronize data between distant sites [23]. We have estimated that the phase noise between the two propagation directions on fiber loop (F1+F2) is highly correlated [18,24]. When combining different beat notes mentioned above, the reciprocal noise are removed in the TW observables. The CTW observable Φ_{CTW} only contains the non-reciprocal fiber noise which we will discuss in details.

3. Performance limitations

Here we will discuss the main limiting factor for the performance of the bidirectional two-way setup. The fiber noise cancellation technique is based on the assumption that phase fluctuations are identical for forward and backward directions. However, in an actual frequency transfer fiber link, this assumption will be degraded by the path, frequency, wavelength and polarization asymmetry. In addition, it will also probably be limited by the coherence and frequency drift of the laser source.

At the beginning, we should mention that the radio frequency (RF) phase noise is negligible. As we phase-lock all the reference synthesizers for the beat note tracking and the frequency counter to a common 10 MHz reference signal, the RF electronic noise can be neglected even for very low fiber phase noise. This is also confirmed by replacing the beat notes by the direct output of synthesizers, and the noise level is significantly low. Note that the wavelength-dependent polarization mode dispersion (PMD) effect is negligible, because the laser source we used is ultra-stable. We mention also that the non-reciprocal power could induce non-reciprocal phase noise due to the Kerr effect. However, this non-reciprocal phase noise is also negligible compared to other limitations discussed here [11].

3.1. Laser source frequency drift

In classical two-way method, two laser sources are used for each direction which suffers from the drift of their relative frequency difference,

$$\frac{d\Phi_{CTW\text{-}1}}{dt} = \left\{ \left[v_2(t) - v_1(t) \right] + \tau \left[\frac{dv_2(t)}{dt} - \frac{dv_1(t)}{dt} \right] - \tau^2 \left[\frac{d^2v_2(t)}{dt^2} - \frac{d^2v_1(t)}{dt^2} \right] \right\}. \tag{5}$$

With typical values of $\frac{dv(t)}{dt} \sim 1\,\mathrm{Hz/s}$ and $\frac{d^2v(t)}{dt^2} \sim 1\,\mathrm{Hz/s^2}$, and $\tau \sim 2 \times 10^{-4}$ s with 43 km fiber link, the long-term instability will be limited to be $\sim 10^{-19}$ [21].

When the laser sources are set in common mode, e.g. in our case, the same laser is used in the two directions, thus the instability arising from the drift of laser source can be largely rejected. In our setup, the ultra-stable laser is referencing its frequency to an H-maser using an optical frequency comb and an offset-phase locked laser. The laser frequency drift is $\sim 10\,\mathrm{mHz/s}$ and therefore its contribution to the uncertainty of CTW observable is negligible.

3.2. Frequency and wavelength asymmetry

In order to reduce stray reflection effect and distinguish beat notes, we usually use different driving frequencies for AOMs. As a result, the forward and backward signals propagate via the optical fiber with a frequency asymmetry of v_{asym}. In our CTW observable, v_{asym} = 224 MHz, this frequency asymmetry results in an imperfect phase noise cancellation, because a delay change corresponds to different phase variations for the forward and backward signals [25],

$$\Phi_{CTW\text{-}2} \approx \frac{v_{asym}}{v_0} \times \Phi_{1+2} \approx 1 \times 10^{-6} \Phi_{1+2}. \tag{6}$$

where v_0 is the frequency of the optical carrier. Thus, the instability of the CTW observable is then

$$\sigma_{CTW} \approx 1 \times 10^{-6} \sigma_{1+2}. \tag{7}$$

This frequency asymmetry effect limits the CTW observable instability to around 1×10^{-6} of the free-running link instability. As the uncertainty of the RF signal applied to the AOMs is <1 mHz, its contribution to the uncertainty of CTW observable is also negligible.

This frequency asymmetry ν_{asym} also causes an imperfect phase noise cancellation due to the chromatic dispersion of SMF-28 fiber, which is $D(\lambda) \sim 17$ ps/(nm·km) at 1542 nm. For the frequency asymmetry $\nu_{\text{asym}} = 224$ MHz, the corresponding wavelength asymmetry $\lambda_{\text{asym}} \approx 0.0018$ nm, then

$$\Phi_{\text{CTW-3}} \approx D(\lambda)\lambda_{\text{asym}}\frac{c}{n} \times \Phi_{1+2} \approx 1 \times 10^{-8}\Phi_{1+2}. \tag{8}$$

Clearly, compared to frequency asymmetry effect, the wavelength asymmetry effect is two orders of magnitude lower and is negligible. Uncertainties on the chromatic dispersion coefficient, the effective refractive index and the wavelength of the laser contribute to the uncertainty of the wavelength asymmetry effect. Among them, the uncertainty on the chromatic dispersion coefficient $D(\lambda)$ is dominant. We assume here that $D(\lambda)$ is known with an uncertainty of $\approx 10\%$, so the uncertainty of the wavelength asymmetry is set to 10% of the total effect.

3.3. Interferometer noise

Temperature variation acts both on the fiber physical length and the fiber index. Around the working temperature T_0, the thermal fiber noise density can be expressed as [22]:

$$\delta\phi(z,t) = \frac{n(T_0)}{c}(\alpha + \xi) \cdot \Delta T(z,t). \tag{9}$$

where $n(T_0) = 1.468$ is the fiber refraction index, $\alpha = \frac{1}{L}\frac{\partial L}{\partial T}$ is the fiber linear thermal expansion coefficient ($\sim 0.55 \times 10^{-6}$ K^{-1} for silica), $\xi = \frac{1}{n}\frac{\partial n}{\partial T}$ is the thermo-optic coefficient ($\sim 7 \times 10^{-6}$ K^{-1} for silica-core fiber), ΔT is the temperature variation in the interferometers. Clearly, the refraction index variation with temperature is by far the dominant effect. Here we conveniently express the phase error as a time error in femtosecond. For SMF28 fiber specifications, we obtain a phase-temperature coefficient $\gamma = \frac{n(T_0)}{c}(\alpha + \xi) \approx 37$ fs/(K·m) for an optical carrier at 194.4 THz and at $T_0 = 298$ K [22].

Note that these thermal variations which affect the non-common fibers are quasi-static compared to the propagation delay in the fiber link. Thus, the total thermal phase variation for CTW observable, which is so-called interferometer noise, can be simply expressed as

$$\Phi_{\text{CTW-4}}(t) = \gamma \cdot \Delta L \cdot \Delta T(t). \tag{10}$$

where ΔL is the length mismatch. The physical length mismatch δL reads as $\delta L = L_{\text{CD}} + L_{\text{OA}} + L_{\text{AB}} - L_{\text{OC}} \approx 0.15$ m [18,21]. The asymmetry of the interferometer will affect the CTW observable discussed here as $\Delta L = 2\delta L \approx 0.3$ m (see Fig. 1 for the definition of point O, A, B, C and D).

To minimize the interferometer noise, the passive strategy is to measure as precisely as possible the relevant non-common optical lengths and the temperature evolution of the interferometers, and compensate this part of the interferometer noise by post-processing [19]. The active strategy is to minimize the relevant non-common fiber lengths and actively stabilize the temperature of the interferometers.

A relative frequency bias exists due to the temperature drift of the interferometer ensemble and reads as $\gamma \cdot \Delta L \cdot \frac{d\Delta T}{dt}$, and the uncertainty is governed by the uncertainty of the temperature measurement. In our setup, the temperature change is about -2.3×10^{-8} K/s. Calculating the derivative of the out-of-loop temperature data and using Eq. (10), we obtain an estimate of the relative frequency bias of -2.6×10^{-22} for the data shown in next section. The standard

deviation of the temperature is estimated in our setup as the mean of two out-of-loop temperature sensors set in the interferometer box. The temperature fluctuation deviation is estimated as 2 mK over 5 days that sets an upper limit for the achieved temperature control. Calculating the long-term Overlapping Allan deviation (OADEV) of the interferometer contribution, we obtain an uncertainty of 1×10^{-22} for the CTW observable with a data set of 392 thousands of seconds (see next section).

3.4. *Polarization asymmetry*

Single mode fiber sustains only one mode of propagation, however, suffers from dispersion called polarization mode dispersion (PMD). Even though we call the fiber 'single mode', it actually carries two modes. Due to birefringence, the refractive-index of the two modes orthogonally polarized at the two principle axes of a bent fiber will differ from each other. Single mode optical fibers do not normally preserve the polarization state of the light propagating along the fiber. The birefringence-induced polarization fluctuations and polarization mode dispersion are varying in time because of the mechanical stress induced by vibrations or by temperature and relative humidity (RH) fluctuations. The polarization state of the light in the fiber is very sensitive to any perturbation which is not symmetric with respect to the fiber axis. Thus, the polarization of the forward and backward transmitted signals changes and leads to changes of the propagation delay asymmetry.

This birefringence-induced polarization noise is a non-reciprocal noise, that cannot be compensated in the closed-loop stabilization system and it degrades the noise compensation and could also introduce a systematic bias in the forward noise measurement. We will refer later on to this effect as polarization noise (PN).

Using n_x and n_y defined as the effective refractive-index of two polarization eigen modes along the fast and slow axes, the phase difference between the two orthogonally polarized modes can be expressed as,

$$
\begin{aligned}
\delta\phi_{\text{PMD}}(z,t) &= \frac{n_x - n_y}{c}\left[(\alpha + \xi) \cdot \Delta T(z,t) + \beta \cdot \Delta RH(z,t)\right] \\
&= B_{xy} \cdot \left[S_{\text{T}} \cdot \Delta T(z,t) + S_{\text{RH}} \cdot \Delta RH(z,t)\right],
\end{aligned}
\tag{11}
$$

where S_{T} and S_{RH} are the sensitivities to temperature and relative humidity, respectively. ΔT and ΔRH are the changes in temperature and relative humidity accordingly. $B_{xy} = (n_x - n_y)/\sqrt{n_x n_y}$ is the birefringence, typically in the order of $10^{-7} < B_{xy} < 10^{-5}$ for commonly available single mode fibers [26]. β is the hygroscopic longitudinal expansion coefficient (1.58×10^{-6} %RH^{-1}) [27]. The temperature sensitivity is $S_{\text{T}} \approx \gamma \approx 37$ fs/(K·m). The relative humidity sensitivity is $S_{\text{RH}} = \beta \cdot \sqrt{n_x n_y}/c \approx 7.7$ fs/(%RH·m).

Then, the total PN phase variation along the spooled fiber for CTW observable can be expressed as

$$
\Phi_{\text{CTW-5}}(t) = B_{xy} \cdot \int_A^C \left[S_{\text{T}} \cdot \Delta T(z,t) + S_{\text{RH}} \cdot \Delta RH(z,t)\right] \mathrm{d}z.
\tag{12}
$$

This model supposes that temperature and relative humidity are independent. In case of strong correlations between these variables, alternative model can be better (see Eq. (15) in Sec. 4).

As a matter of fact, a degraded stability of RF frequency transfer due to non-reciprocal noise caused by PMD in the optical fiber has already been reported in the literature and a solution has been proposed to scramble the polarization rapidly to average out the PMD effect [28–30]. However, the effect of PMD and polarization fluctuation has never been observed in the optical carrier frequency transfers, to the best of our knowledge. This is due to the fact that the actuator (an AOM) causes much less polarization variation of the optical signals

than the fiber stretcher used for the RF modulation frequency transfer. On the other hand, the standard telecommunication fiber networks are buried in the ground, and well fixed and isolated. Consequently, PMD fluctuations of the in-field fiber link are slow, and their effect is negligible [7]. It is noticeable that fiber spools provide us a good opportunity to study this polarization noise in optical frequency transfer because it is exaggerated in fiber spools which experience more mechanical stress and temperature fluctuations, and because of the coherent excitation of the fiber link as the spools are located in one single site. In addition, the temperature and relative humidity variations are monitored for the whole link, so we can analyze this polarization noise quantitatively.

3.5. Propagation delay

Due to the propagation delay, the maximum noise rejection is given by

$$S_{\text{CTW}}(f) = \frac{(\tau_1 + \tau_2)^2}{3}(2\pi f)^2 S_{12}(f). \tag{13}$$

where $S_{12}(f)$ is the power spectrum density (PSD) of the one-way fiber noise, and it has been assumed that the fiber noise is uncorrelated with position [12]. It gives a limit which is lower than the current noise floor.

However, it is interesting to note that in our spooled fibers, considering that the fiber noise is arising from optical length variations induced by temperature variation, thus it could be correlated on a length given by the perimeter P of the spools. The limit becomes:

$$S_{\text{CTW}}(f) = \frac{(L_1 + L_2)}{P}\frac{(\tau_1 + \tau_2)^2}{3}(2\pi f)^2 S_{12}(f). \tag{14}$$

With $(L_1 + L_2)/P \approx 10^5$, it gives a limit $S_{\text{CTW}}(f) = 0.08f^2 S_{12}(f)$ which is higher than the current noise floor.

It shows that the fiber noise is partly uncorrelated with position. This is expected result as the typical length for the birefringence variation (polarization beat length) is greater than the perimeter of the spools. In addition, since the fiber birefringence changes randomly along the fiber, one expects a scaling of the PN contribution to $S_{12}(f)$ with the optical fiber link length.

4. Experimental results

4.1. Optical phase noise

The experiments were carried out on spooled fibers with length of $\sim 25\,\text{km}$ for F1 and F2 each. The two fiber spools have the same propagation delay within 1.5 ns, that we cross-checked with a time transfer experiment. Assuming an effective index of refraction $n = 1.4682$, the total looped fiber optical length is $L = L1 + L2 = 50\,776\,\text{m}$ for the free running one-way signal, as measured with an optical time domain reflectometer (OTDR). The resolution of the measurement is below 1-m. The inaccuracy is evaluated as $\pm 10\,\text{m}$, mainly given by the inaccuracy of the index of refraction. The fiber spools are connected in such a way that the normal vectors to the enclosed surfaces of each spool are opposite in direction (see Fig. 1). The total enclosed area of the two spools is therefore close to 0, and no phase fluctuation can arise from coupling of the enclosed area with the Earth rotation rate.

The green and black lines shown in Fig. 2(a) are the integrated optical phases of the free running one-way signals Φ_{1+2} and Φ_{2+1}. For sake of clarity, we only show Φ_{1+2} and Φ_{2+1}, because Φ_{1+1} and Φ_{2+2} follow almost the same trace. Based on Eq. (9), we can estimate the temperature related noise for a fiber loop with a length of 50 776 m, as shown in Fig. 3(a) (green dashed line). We note that the phase evolution of free running one-way shows significantly high correlation (95.8%) with the temperature variation in Lab2 where the fiber spools are located, as

displayed on Fig. 4(b). This temperature variation induces fiber length and fiber index changes for our spooled fiber. It confirms that the free running one-way signal is dominated by the fiber noise induced by the environmental fluctuation, here specially the temperature variation. It confirms that the underlying assumption of thermal equilibrium between the room temperature and the fiber spools is reached at relevant time scale.
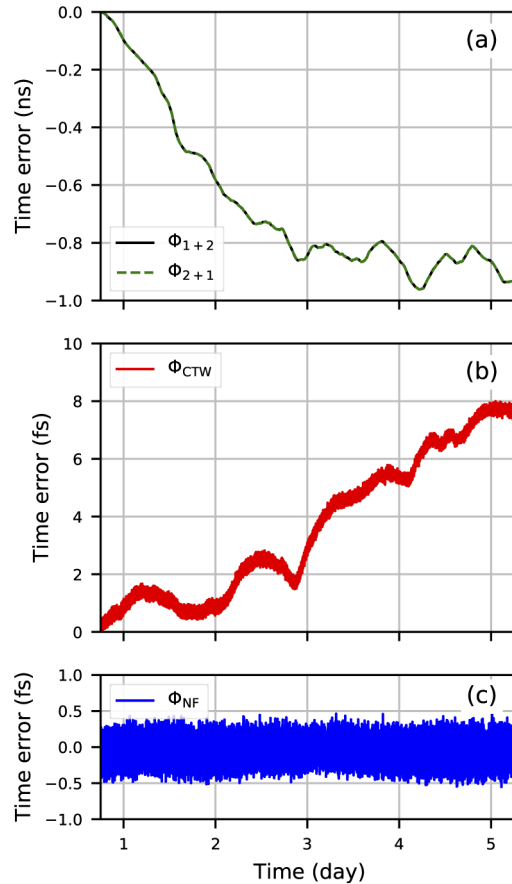

Fig. 2. Phase evolution of (a) free running one-way signal (Φ_{1+2} and Φ_{2+1}), (b) classical two-way (CTW) observable (Φ_{CTW}), and (c) noise floor (NF) in-situ (Φ_{NF}).

The phase evolution of the CTW observable Φ_{CTW} is shown in Fig. 2(b) (red line). In this experiment, the temperature inside the interferometer ensemble is actively stabilized. The temperature data are gathered from the sensors out-of-loop every 10 seconds and its variation ΔT_{interf} is less than 10 mK in 5 days. Based on Eq. (10), with a length mismatch of $\Delta L = 0.3$ m in the interferometers, the interferometer noise $\gamma \cdot \Delta L \cdot \Delta T_{interf} \leq 0.1$ fs, as shown in Fig. 3(b) (green dashed line). We note that the interferometer noise cannot account for the phase noise Φ_{CTW} (~ 8 fs over 5 days). When the temperature is stabilized in the interferometer, the interferometer noise is negligible and some other factors must exist to dominate the CTW observable.

Moreover, the blue line in Fig. 2(c) shows the phase evolution of the noise floor in-situ. It fluctuates only in the range of ± 0.5 fs. It is not relevant to the environmental temperature and relative humidity fluctuations both in Lab1 and Lab2, so it is free of not only the interferometer noise but also the polarization noise. It is the noise floor of our setup.
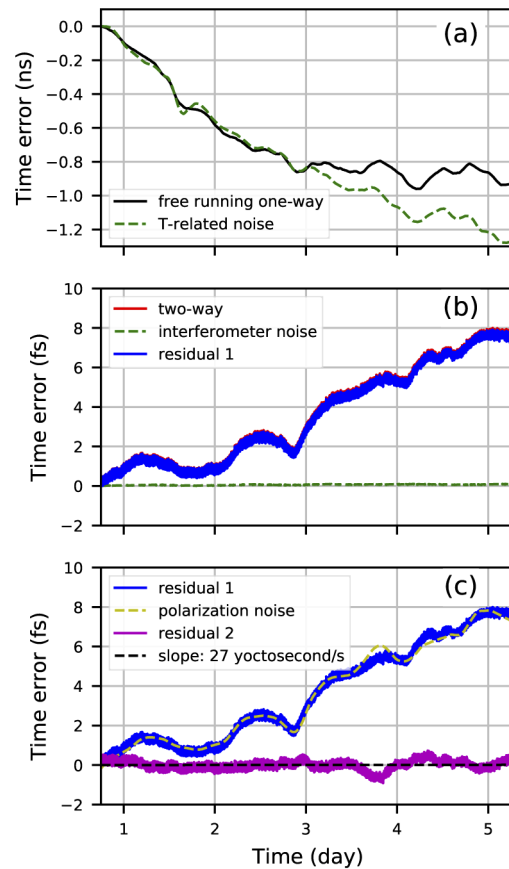
Fig. 3. (a) Phase evolution of the free running one-way signal and the temperature related noise in Lab2, (b) phase evolution of the CTW observable, interferometer noise and the residual 1, (c) polarization noise and the residual 2.
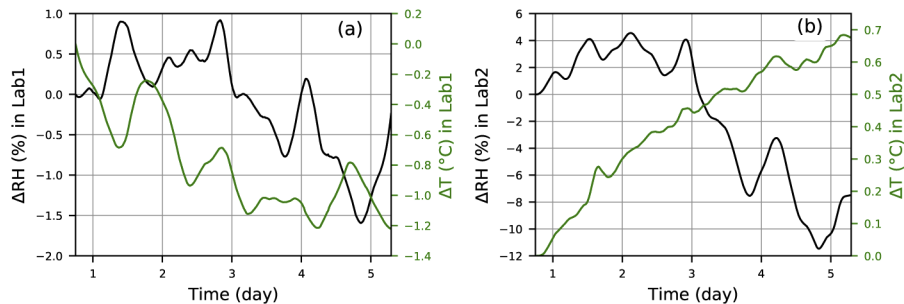

Fig. 4. The temperature and relative humidity variations (a) in Lab1 (ΔT_1, ΔRH_1) and (b) in Lab2 (ΔT_2, ΔRH_2).

In this study we measured the room temperature and relative humidity both in Lab1 and Lab2. Their variations are shown in Fig. 4. The correlation coefficients between the phase evolution Φ_{CTW} and the temperature and relative humidity variations (ΔT_1, ΔRH_1, ΔT_2, ΔRH_2) are listed in Table 1. As the major part ($\sim 50\,576$ m) of the spooled fiber link is located in Lab2 and a minor part (~ 200 m) in Lab1, higher correlations (91% and -93%) are observed between the

phase evolution of the CTW observable Φ_{CTW} and the temperature variation ΔT_2 and the relative humidity variation ΔRH_2 measured in Lab2, lower correlations with ΔT_1 (-82%) and ΔRH_1 (-84%) in Lab1. Thus, we attribute the optical phase evolution of CTW to polarization noise induced not only by temperature fluctuations but also by relative humidity fluctuations impacted on spooled fibers.

Table 1. Correlation coefficients between the phase evolution of CTW observable and the temperature and relative humidity variations both in Lab1 and Lab2.

	ϕ_{CTW}	ΔT_1	ΔRH_1	ΔT_2	ΔRH_2
ϕ_{CTW}	1.0	-0.82	-0.84	0.91	-0.93
ΔT_1	-0.82	1.0	0.44	-0.86	0.60
ΔRH_1	-0.84	0.44	1.0	-0.65	0.93
ΔT_2	0.91	-0.86	-0.65	1.0	-0.75
ΔRH_2	-0.93	0.60	0.93	-0.75	1.0

Based on Eq. (12), we can estimate the non-reciprocal polarization noise, but the birefringence of our spooled fiber B_{xy} is unknown. We use a multi-linear fitting procedure to fit the CTW observable. Because of moderately high correlations between the temperature variation and relative humidity variation in our experiment, the lower residuals are obtained with the following model

$$\Phi_{CTW-5}(t) = B_{xy} \cdot \int_A^C \left\{ S_T \cdot \Delta T(z,t) \left[1 + \epsilon \cdot \Delta RH(z,t) \right] \right\} dz. \qquad (15)$$

It shows that relative humidity changes the thermal conductivity and therefore enhances the sensitivity to temperature variations. The fitted parameter of birefringence for the major 50 576 m of the spooled fiber link is $B_{xy} \approx 1.4 \times 10^{-6}$ with $\epsilon \approx 0.16$, for the minor 200 m fiber is $B_{xy} \approx 3.6 \times 10^{-4}$ with $\epsilon \approx 0.28$. The 200 m fiber has an additional polymer-coating as compared to the fiber spools, and exhibits higher sensitivities to temperature and relative humidity variations. The fitted polarization noise is shown in Fig. 3(c) (yellow dashed line). After removing the polarization noise from the CTW observable, we obtain the residual noise within ±1 fs, as shown in Fig. 3(c) (pink line). The linear drift of the residual phase, which is as low as 27 yoctosecond/s, is within the residual noise fluctuations and is not significant. This residual noise may be due to imperfect temperature and humidity sensing.

4.2. Phase noise power spectral density (PSD)

Considering standard random signal processing, the fiber phase noise power spectral density is given by the Fourier transform of the auto-correlation function of its phase noise [22].

Figure 5 shows the phase noise PSD of free running one-way, CTW observable, noise floor in-situ, as well as the residual of CTW after removing the interferometer noise and polarization noise. For the free running one-way signal $S_{12}(f)$, it falls off as a flicker frequency noise ($\propto f^{-3}$) over all the Fourier frequency range. The $S_{CTW}(f)$ behaves as white phase noise and flicker phase noise ($\propto f^0$ and f^{-1}) for Fourier frequency $f \geq 4 \times 10^{-4}$ Hz, and as flicker frequency noise ($\propto f^{-3}$) for Fourier frequency $f \leq 10^{-4}$ Hz. The blue curve in Fig. 5 indicates the noise floor in-situ which shows flicker phase noise signature over almost the full frequency range.

For high Fourier frequency ($f \geq 10^{-3}$ Hz), the noise level of CTW $S_{CTW}(f)$ is very close to that of the noise floor in-situ. For low Fourier frequency ($f \leq 10^{-3}$ Hz), compared to the one-way free running, the fiber noise is rejected by $\sim$ 10 orders of magnitude in the CTW observable; moreover, compared to the noise floor in-situ, the CTW observable still have some extra noise. In Ref. [19], the extra noise at low frequency was dominated by the interferometer noise where
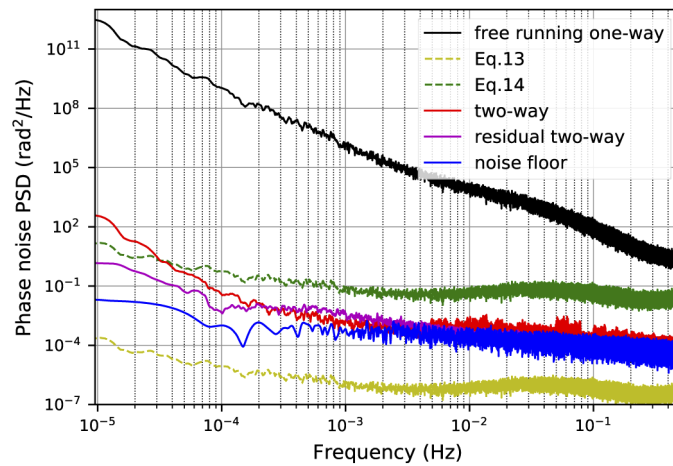
Fig. 5. Phase noise power spectral density (PSD) of the free running one-way signal (black), the classical two-way (CTW) observable (red), its residual after removing interferometer and polarization noise (pink), the noise floor in-situ (blue). The yellow and green lines show the limits due to the propagation delay without and with correlations, corresponding to Eqs. (13) and (14) respectively.

the correlation between the phase evolution and temperature variation in the interferometers was confirmed as high as 98.6%. Then the interferometer noise was evaluated and further removed by data post-processing. In this experiment with active stabilization of the temperature inside the interferometer box in Lab1, the interferometer noise is minimized in-situ. Therefore, the CTW residual noise at lower frequencies are originating from polarization noise arising from the spooled fibers. After removing this polarization noise by data post-processing, it drops to the pink curve in Fig. 5, which further confirms that the polarization noise dominates the CTW observable at low Fourier frequencies.

4.3. Frequency stability estimated as Modified Allan Deviation (MDEV)

The MDEV of the free-running one-way noise, the two-way observable and noise floor in-situ are shown in Fig. 6. The MDEV of the two-way observable starts from 5×10^{-17} at integration time $\tau = 1$ s and decreases to 3×10^{-20} at integration time $\tau = 1000$ s, then shows a plateau at integration time $\tau > 1000$ s. The MDEV of noise floor starts from 8×10^{-17} at integration time $\tau = 1$ s and decreases directly to 3×10^{-22} at integration time $\tau = 10^5$ s. We notice that the stability of noise floor is higher than that of CTW observable at integration time $<10^3$ s. This is because the noise floor is indeed a combination of 4 beat notes with higher detection shot noise, whereas the CTW is a combination of 2 beat notes.

For in-field fiber link, the discrepancy between two-way and noise floor at long timescales is due to the interferometer noise [18,19]. For spooled fiber link in the lab, this discrepancy is mainly due to the polarization noise. With active temperature stabilization in the interferometer box, the instability of the interferometer is at a very low level (green dashed line in Fig. 6). The instability of CTW at long-term is explained by the polarization noise, as shown in Fig. 6 (yellow dashed line). It is degraded by the temperature and relative humidity changes impacted on the spooled fibers. The expected instability of residual two-way (pink star) indicates that ultimate instability would reach 10^{-21} within a few days integration time, assuming interferometer noise and polarization noise rejection.
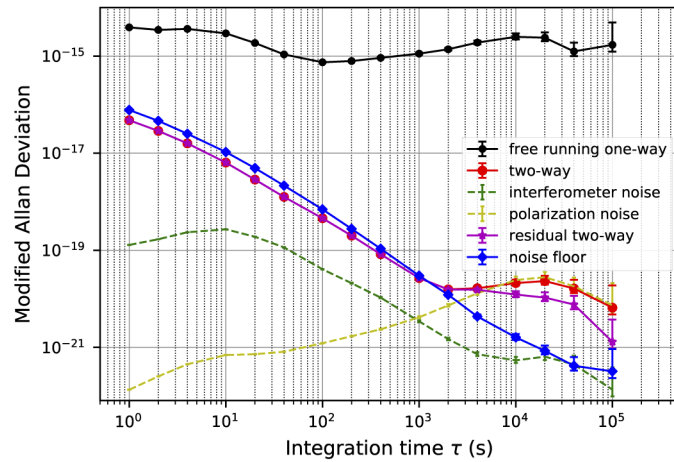
Fig. 6. Fractional frequency instability expressed as modified Allan deviation (MDEV) for free running one-way (black circle), two-way observable (red circle) , interferometer noise (green, dashed), polarization noise (yellow, dashed), residual two-way after removing interferometer and polarization noise (pink star), and noise floor in-situ (blue diamond).

4.4. Accuracy budget

We evaluate the uncertainty contributions of the above listed effects and physical model to the uncertainty budget of a coherent fiber link, by calculating the systematic offset (systematic bias). Their associated uncertainty (systematic uncertainties, type B) are evaluated from the experimental control of the parameters (as laser drift, frequency control and temperature control). For the polarization noise term, it can be computed using Eq. (15). The room temperature and relative humidity where the spools sits were measured during the experiment (Fig. 4). It found an excursion of temperature about 700 mK and relative humidity about 16 %RH over ~5 days. With $\gamma = 37$ fs/K/m and the fitted $B_{xy} \approx 1.4 \times 10^{-6}$, we obtain a frequency bias of 1.9×10^{-20}. This value strongly depends on the effective birefringence of the spooled fiber. It is resulting from a fit of experimental data and is significantly dependent on the fiber and manufacturing process (see section above). So we evaluate its uncertainty as the long-term OADEV of the polarization induced optical phase fluctuation (blue trace in Fig. 3), and report it as the polarization noise induced bias and uncertainty. Reciprocally, this value can be interpreted as a measure of the fiber birefringence, which is $B_{xy} \approx 1.4 \times 10^{-6}$ for our pair of fiber spools.

Table 2 lists the major frequency shifts and their related uncertainties that affect our setup. The two-way scheme on spooled fiber link is dominated by polarization noise with systematic

Table 2. Accuracy budget of the presented 50-km spooled fiber link.

Effect	Bias ($\times 10^{-20}$)	uncertainty ($\times 10^{-20}$)
Local oscillator	$<10^{-5}$	$<10^{-5}$
Laser drift	0	0
Frequency asymmetry	$<10^{-1}$	$<10^{-12}$
Wavelength asymmetry	$<10^{-3}$	$<10^{-4}$
Interferometer	-2.6×10^{-2}	1×10^{-2}
Polarization asymmetry	1.9	1.2
Total	1.9	1.2

uncertainty of 1.2×10^{-20}. The statistical uncertainty for the CTW observable is 8×10^{-21}. The total uncertainty budget reads as $1.9(\pm 0.8)(\pm 1.2) \times 10^{-20}$. After compensation of the polarization induced asymmetry, we compute the mean and the OADEV (at 10^5 s integration time) of the residual (residual 2 in Fig. 3), and found $2.6(\pm 39) \times 10^{-22}$.

5. Conclusion

We presented the first noise characterization of the laser source, frequency, wavelength, interferometer and polarization asymmetry between the forward and backward propagation signals on optical fibers in two-way method. We observed interactions between temperature variation and relative humidity variation and measured optical phase in a spooled fiber link, and we identified the mechanism behind the observed perturbations. We report here for the first time, to the best of our knowledge, experimental observation of non-reciprocal noise in bi-directional fiber links. These measurements are an essential prerequisite for the best exploitation of two-way fiber links at their fundamental limits as for instance the search for Dark Matter at time constant greater than $1\,000$ s [17], and for the study of more fundamental non-reciprocal noise such as the Sagnac effect that one can expect at the low 10^{-21} level. We showed that, when interferometer noise is minimized by actively stabilizing the temperature of the interferometers, the PMD noise will dominate the low Fourier frequencies for experiments on spooled fibers, and can be compensated in post-processing using its correlations with temperature and humidity variations. This strategy is shown to be effective on a fiber-spools experiment. This work lays the basis of understanding polarisation effects in optical fiber link and opens the way for better interferometer designs, higher sensitive experiment with specific fibers [31–33], and other mitigation strategies for in-field applications of time and frequency transfer as polarisation scrambling [20]. Further research on polarization noise control will allow to push the fiber link to a more accurate regime in the $10^{-22} - 10^{-23}$ range.

Disclosures. The authors declare no conflicts of interest.

References

1. J. Ye, J.-L. Peng, R. J. Jones, K. W. Holman, J. L. Hall, D. J. Jones, S. A. Diddams, J. Kitching, S. Bize, J. C. Bergquist, L. W. Hollberg, L. Robertsson, and L.-S. Ma, "Delivery of high-stability optical and microwave frequency standards over an optical fiber network," J. Opt. Soc. Am. B **20**(7), 1459–1467 (2003).
2. A. Yamaguchi, M. Fujieda, M. Kumagai, H. Hachisu, S. Nagano, Y. Li, T. Ido, T. Takano, M. Takamoto, and H. Katori, "Direct comparison of distant optical lattice clocks at the 10^{-16} uncertainty," Appl. Phys. Express **4**(8), 082203 (2011).
3. T. Akatsuka, H. Ono, K. Hayashida, K. Araki, M. Takamoto, T. Takano, and H. Katori, "30-km-long optical fiber link at 1397 nm for frequency comparison between distant strontium optical lattice clocks," Jpn. J. Appl. Phys. **53**(3), 032801 (2014).
4. C. Lisdat, G. Grosche, N. Quintin, C. Shi, S. Raupach, C. Grebing, D. Nicolodi, F. Stefani, A. Al-Masoudi, S. Dörscher, S. Häfner, J.-L. Robyr, N. Chiodo, S. Bilicki, E. Bookjans, A. Koczwara, S. Koke, A. Kuhl, F. Wiotte, F. Meynadier, E. Camisard, M. Abgrall, M. Lours, T. Legero, H. Schnatz, U. Sterr, H. Denker, C. Chardonnet, Y. Le Coq, G. Santarelli, A. Amy-Klein, R. Le Targat, J. Lodewyck, O. Lopez, and P.-E. Pottie, "A clock network for geodesy and fundamental science," Nat. Commun. **7**(1), 12443 (2016).
5. J. Grotti, S. Koller, S. Vogt, S. Häfner, U. Sterr, C. Lisdat, H. Denker, C. Voigt, L. Timmen, A. Rolland, F. N. Baynes, H. S. Margolis, M. Zampaolo, P. Thoumany, M. Pizzocaro, B. Rauf, F. Bregolin, A. Tampellini, P. Barbieri, M. Zucco, G. A. Costanzo, C. Clivati, F. Levi, and D. Calonico, "Geodesy and metrology with a transportable optical clock," Nat. Phys. **14**(5), 437–441 (2018).
6. K. Beloy, M. I. Bodine, T. Bothwell, S. M. Brewer, S. L. Bromley, J.-S. Chen, J.-D. Deschênes, S. A. Diddams, R. J. Fasano, T. M. Fortier, Y. S. Hassan, D. B. Hume, D. Kedar, C. J. Kennedy, I. Khader, A. Koepke, D. R. Leibrandt, H. Leopardi, A. D. Ludlow, W. F. McGrew, W. R. Milner, N. R. Newbury, D. Nicolodi, E. Oelker, T. E. Parker, J. M. Robinson, S. Romisch, S. A. Schäffer, J. A. Sherman, L. C. Sinclair, L. Sonderhouse, W. C. Swann, J. Yao, J. Ye, and X. Zhang, "Frequency ratio measurements with 18-digit accuracy using a network of optical clocks," arXiv:2005.14694 [physics] (2020).

7. C. Clivati, P. Savio, S. Abrate, V. Curri, R. Gaudino, M. Pizzocaro, and D. Calonico, "Robust optical frequency dissemination with a dual-polarization coherent receiver," Opt. Express **28**(6), 8494–8511 (2020).
8. M. I. Bodine, J.-D. Deschênes, I. H. Khader, W. C. Swann, H. Leopardi, K. Beloy, T. Bothwell, S. M. Brewer, S. L. Bromley, J.-S. Chen, S. A. Diddams, R. J. Fasano, T. M. Fortier, Y. S. Hassan, D. B. Hume, D. Kedar, C. J. Kennedy, A. Koepke, D. R. Leibrandt, A. D. Ludlow, W. F. McGrew, W. R. Milner, D. Nicolodi, E. Oelker, T. E. Parker, J. M. Robinson, S. Romish, S. A. Schäffer, J. A. Sherman, L. Sonderhouse, J. Yao, J. Ye, X. Zhang, N. R. Newbury, and L. C. Sinclair, "Optical atomic clock comparison through turbulent air," Phys. Rev. Res. **2**(3), 033395 (2020).
9. I. Ushijima, M. Takamoto, M. Das, T. Ohkubo, and H. Katori, "Cryogenic optical lattice clocks," Nat. Photonics **9**(3), 185–189 (2015).
10. E. Oelker, R. B. Hutson, C. J. Kennedy, L. Sonderhouse, T. Bothwell, A. Goban, D. Kedar, C. Sanner, J. M. Robinson, G. E. Marti, D. G. Matei, T. Legero, M. Giunta, R. Holzwarth, F. Riehle, U. Sterr, and J. Ye, "Demonstration of 4.8 x 10^{-17} stability at 1 s for two independent optical clocks," Nat. Photonics **13**(10), 714–719 (2019).
11. P. A. Williams, W. C. Swann, and N. R. Newbury, "High-stability transfer of an optical frequency over long fiber-optic links," J. Opt. Soc. Am. B **25**(8), 1284–1293 (2008).
12. C. E. Calosso, E. Bertacco, D. Calonico, C. Clivati, G. A. Costanzo, M. Frittelli, F. Levi, A. Mura, and A. Godone, "Frequency transfer via a two-way optical phase comparison on a multiplexed fiber network," Opt. Lett. **39**(5), 1177–1180 (2014).
13. A. Bercy, F. Stefani, O. Lopez, C. Chardonnet, P.-E. Pottie, and A. Amy-Klein, "Two-way optical frequency comparisons at 5 x 10^{-21} relative stability over 100-km telecommunication network fibers," Phys. Rev. A **90**(6), 061802 (2014).
14. C. Clivati, D. Calonico, G. A. Costanzo, A. Mura, M. Pizzocaro, and F. Levi, "Large-area fiber-optic gyroscope on a multiplexed fiber network," Opt. Lett. **38**(7), 1092–1094 (2013).
15. E. Savalle, A. Hees, F. Frank, E. Cantin, P.-E. Pottie, B. M. Roberts, L. Cros, B. T. McAllister, and P. Wolf, "Searching for Dark Matter with an Optical Cavity and an Unequal-Delay Interferometer," Phys. Rev. Lett. **126**(5), 051301 (2021).
16. B. M. Roberts, P. Delva, A. Al-Masoudi, A. Amy-Klein, C. Baerentsen, C. F. A. Baynham, E. Benkler, S. Bilicki, S. Bize, W. Bowden, J. Calvert, V. Cambier, E. Cantin, E. A. Curtis, S. Dörscher, M. Favier, F. Frank, P. Gill, R. M. Godun, G. Grosche, C. Guo, A. Hees, I. R. Hill, R. Hobson, N. Huntemann, J. Kronjäger, S. Koke, A. Kuhl, R. Lange, T. Legero, B. Lipphardt, C. Lisdat, J. Lodewyck, O. Lopez, H. S. Margolis, H. Álvarez Martínez, F. Meynadier, F. Ozimek, E. Peik, P.-E. Pottie, N. Quintin, C. Sanner, L. De Sarlo, M. Schioppo, R. Schwarz, A. Silva, U. Sterr, C. Tamm, R. Le Targat, P. Tuckey, G. Vallet, T. Waterholter, D. Xu, and P. Wolf, "Search for transient variations of the fine structure constant and dark matter using fiber-linked optical atomic clocks," New J. Phys. **22**(9), 093010 (2020).
17. C. J. Kennedy, E. Oelker, J. M. Robinson, T. Bothwell, D. Kedar, W. R. Milner, G. E. Marti, A. Derevianko, and J. Ye, "Precision Metrology Meets Cosmology: Improved Constraints on Ultralight Dark Matter from Atom-Cavity Frequency Comparisons," Phys. Rev. Lett. **125**(20), 201302 (2020).
18. D. Xu, W.-K. Lee, F. Stefani, O. Lopez, A. Amy-Klein, and P.-E. Pottie, "Studying the fundamental limit of optical fiber links to the 10 $^{-21}$ level," Opt. Express **26**(8), 9515–9527 (2018).
19. D. Xu, P. Delva, O. Lopez, A. Amy-Klein, and P.-E. Pottie, "Reciprocity of propagation in optical fiber links demonstrated to 10 $^{-21}$," Opt. Express **27**(25), 36965–36975 (2019).
20. D. Xu, O. Lopez, A. Amy, and P.-E. Pottie, "Polarization scramblers to solve practical limitations of frequency transfer," J. Lightwave Technol. (2021).
21. W.-K. Lee, F. Stefani, A. Bercy, O. Lopez, A. Amy-Klein, and P.-E. Pottie, "Hybrid fiber links for accurate optical frequency comparison," Appl. Phys. B **123**(5), 161 (2017).
22. F. Stefani, O. Lopez, A. Bercy, W.-K. Lee, C. Chardonnet, G. Santarelli, P.-E. Pottie, and A. Amy-Klein, "Tackling the limits of optical fiber links," J. Opt. Soc. Am. B **32**(5), 787–797 (2015).
23. A. Tampellini, C. Clivati, F. Levi, A. Mura, and D. Calonico, "Effect of a timebase mismatch in two-way optical frequency transfer," Metrologia **54**(6), 805–809 (2017).
24. S. Koke, A. Kuhl, T. Waterholter, S. M. F. Raupach, O. Lopez, E. Cantin, N. Quintin, A. Amy-Klein, P.-E. Pottie, and G. Grosche, "Combining fiber Brillouin amplification with a repeater laser station for fiber-based optical frequency dissemination over 1400 km," New J. Phys. **21**(12), 123017 (2019).
25. H. Jiang, "Development of ultra-stable laser sources and long-distance optical link via telecommunication networks," Ph.D. thesis, Université Paris 13 (2010).
26. S. Rashleigh, "Origins and control of polarization effects in single-mode fibers," J. Lightwave Technol. **1**(2), 312–331 (1983).
27. L. Men, P. Lu, and Q. Chen, "A multiplexed fiber Bragg grating sensor for simultaneous salinity and temperature measurement," J. Appl. Phys. **103**(5), 053107 (2008).
28. O. Lopez, A. Amy-Klein, C. Daussy, C. Chardonnet, F. Narbonneau, M. Lours, and G. Santarelli, "86-km optical link with a resolution of 2 x 10^{-18} for RF frequency transfer," Eur. Phys. J. D **48**(1), 35–41 (2008).
29. K. Turza, P. Krehlik, and Ł. Śliwczyński, "Stability Limitations of Optical Frequency Transfer in Telecommunication DWDM Networks," IEEE Trans. Ultrason., Ferroelect., Freq. Contr. **67**(5), 1066–1073 (2020).
30. L. Śliwczyński, P. Krehlik, and M. Lipiński, "Optical fibers in time and frequency transfer," Meas. Sci. Technol. **21**(7), 075302 (2010).

31. M. Wada, S. Okubo, F.-L. Hong, and H. Inaba, "Detection and evaluation of fiber noise induced in ultra-stable environments," in *2018 Conference on Precision Electromagnetic Measurements (CPEM)*, (IEEE, 2018), pp. 1–2.

32. B. Rauf, M. C. Vélèez Lopez, P. Thoumany, M. Pizzocaro, and D. Calonico, "Phase noise cancellation in polarisation-maintaining fibre links," Rev. Sci. Instrum. **89**(3), 033103 (2018).

33. E. Cantin, M. Tønnes, R. L. Targat, A. Amy-Klein, O. Lopez, and P.-E. Pottie, "An accurate and robust metrological network for coherent optical frequency dissemination," New J. Phys. (to be published).